Eur. Phys. J. D **37**, 209–215 (2006)
DOI: 10.1140/epjd/e2005-00285-3

THE EUROPEAN PHYSICAL JOURNAL D

Study of Mn laser ablation in methane atmosphere

N. Krstulović, I. Labazan, and S. Milošević[a]

Institute of Physics, P.O. Box 304, 10000 Zagreb, Croatia

Received 8 September 2004 / Received in final form 4 July 2005
Published online 25 October 2005 –

Abstract. Laser ablation of Mn target in vacuum and in the presence of CH_4 was studied under 308 nm laser irradiation. Time-resolved emission using gated detection and scanning monochromator and absorption using the cavity ring-down spectroscopy were used to study vaporized plume. In the CH_4 atmosphere we observed transitions identified as C_2 and MnH bands, while these spectral features were not detected in emission spectra. This is a clear evidence of importance in combining both spectroscopic techniques in laser vaporized plume study.

PACS. 52.38.Mf Laser ablation – 33.20.Kf Visible spectra

1 Introduction

Focusing a laser light on solid target surface results with the hot and dense plasma plume created above the target, in which many relaxation mechanisms lead to the emission of characteristic atomic or molecular spectral lines. Interaction of vaporized material with reactive background may lead to formation of interesting gas-phase molecules and/or ions hardly observed and produced in usual ovens or discharge setups. Laser vaporization has also been used for controllable thin film growing, particularly in recent years for high T_c superconductor film deposition. Standard method for fast quantitative and qualitative analysis of laser induced plume is Laser Induced Breakdown Spectroscopy (LIBS) [1]. However for detection of ground state atoms and molecules laser induced fluorescence or absorption techniques, such as the cavity ring-down spectroscopy (CRDS) have to be used [2,3]. Usefulness in a combined study by CRDS and LIBS was demonstrated recently [4], in study of the morphology of a laser-produced aerosol plume.

There have been several studies of laser ablation of pure manganese or manganese containing samples performed for a purpose of the growth of thin superconducting films. Ground state Mn atoms generated by laser ablation of pure manganese sample were resonantly excited and ionized, and velocity distribution was determined by analyzing temporal evolution of ionic signals [5]. Lecoeur et al. [6] have measured both wavelength- and time-resolved emission of laser induced plume from Mn and Mn_2O_3 targets, in O_2 and N_2O atmosphere. They measured peak velocities of Mn atoms ranging from approx. 1.5×10^6 cm/s for zero pressure, down to 0.3×10^6 cm/s for 0.3 Torr of the background gas. Dang et al. [7] have measured time-resolved mass spectra of neutral and ionic species in the ablation plume of the La–Ca–Mn–O pellets: estimated kinetic energies of ablated metal ions and neutrals were in the range 6–10 eV and 0.2–0.9 eV, respectively, for 355 nm and 532 nm laser beams with 1.5 J/cm^2 laser fluences. Importance of small manganese containing molecules and Mn atoms itself, is evident from their appearance in catalytic processes as well as in mercury–manganese stars [8].

In the present work we have studied both, emission and absorption, of manganese laser ablation plume in vacuum and in the presence of methane gas with the purpose to characterize the plume content in the reactive environment and make comparative observations. Paper is organized as follows. After short description of our laser ablation set-up, we presented emission and absorption measurements results. Discussion and conclusion are given in Sections 4 and 5, respectively.

2 Experiment

For a purpose of the present work we have combined experimental set-ups for the optical emission spectroscopy and for the cavity ring-down spectroscopy, previously described in more details in references [9,10], respectively. Briefly, a manganese plume was induced by a nanosecond 308 nm excimer laser light focused on the Mn target (99.99% purity). Laser ablation was performed in vacuum (less than 10^{-3} Torr) using a roots pump system, or under constant flow of methane, at pressure of few Torr.

[a] e-mail: slobodan@ifs.hr

Precise positioning of the target and lens for focusing excimer laser light was assured by a stepping motors. Target holder was rotating slowly to avoid drilling. We use the cavity ring-down spectroscopy for absorption measurements in the wavelength range (472–485) nm. Prior to the experiment, we tested our cavity ringdown spectrometer which shows no significant change of mirror reflectivity within given wavelength range. Cavity mirrors were mounted directly on the vacuum chamber, in the direction perpendicular to the plume propagation. Finesse of the resonator was about 5200. Detection and analysis of the time-dependent absorption was performed according to the procedure described in [10].

To measure emission spectra, visible photons from the whole ablation plume were focused onto the 6 mm entrance of the optical fiber placed at 35° from the cavity axis. The other part of fiber was mounted on the entrance slit of a 60 cm scanning monochromator with spectral resolution of about 0.1 nm. Wavelength resolved emission was detected by a photomultiplier and measured by means of a boxcar averager for chosen delay and gate settings. That allowed us to study the time evolution of the complete ablation plume emission. To measure the time evolution of signal at particular wavelength, we used a 8 bit 150 MHz digital oscilloscope.

Chosen wavelength interval is of particular interest, since many Mn atomic transition, C_2 and possible MnH rovibrational bands are expected to be observed.

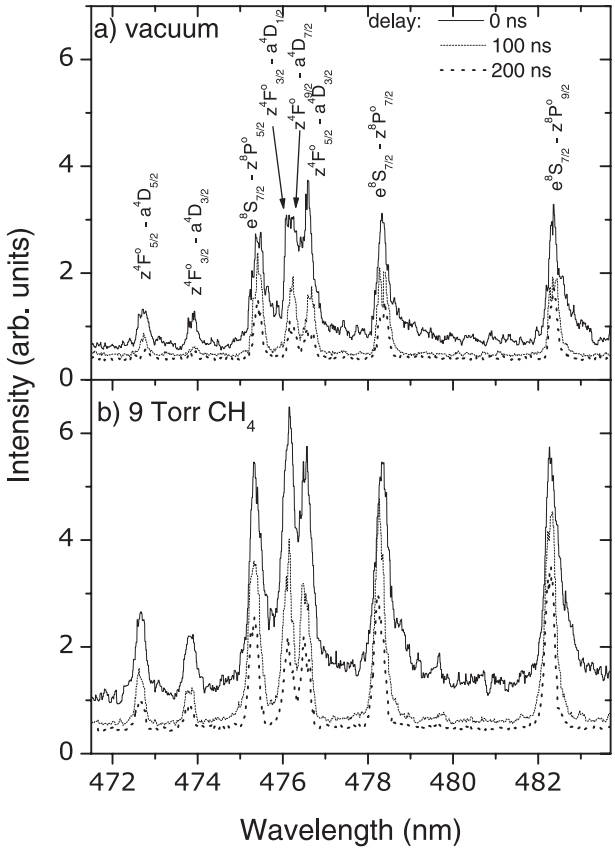

Fig. 1. Time-resolved emission spectra of manganese ablation plume in (a) vacuum and (b) 9 Torr of CH_4, in the wavelength range (471.5–483.7) nm. Boxcar settings were: gate = 200 ns and delays = 0 ns, 100 ns, 200 ns, showed by solid, dashed and dotted lines, respectively. Identification of Mn atomic transitions observed in spectra is indicated in the upper part of figure.

3 Results

3.1 Emission measurements

We recorded emission spectra in the visible wavelength region, 400–700 nm, in vacuum and CH_4 atmosphere. Apart from numerous pronounced manganese atomic line transitions, many low-intensity manganese ions emission lines were observed. In what follow, we present emission spectra measured in smaller wavelength interval, which might be directly compared to absorption measurements showed below.

Figure 1 shows temporal evolution of the manganese plume emission occurring in the wavelength range (471.5–483.7) nm. Gate was set to 200 ns and delays 0 ns (solid line), 100 ns (dash) and 200 ns (dot, bold). Figure 1a shows spectra taken in vacuum and Figure 1b spectra in the presence of 9 Torr of methane. As one can see, we observed only atomic manganese lines, both in vacuum and CH_4. Identification of manganese lines is given in Figure 1a. All identified transitions are between excited Mn atomic levels. The background continuum, intensities and linewidths of all observed lines were decreasing with increasing time delay. Level of this broadband radiation is higher for the laser ablation in the presence of CH_4 than in vacuum by factor of two.

Figure 2 shows the Mn($e^8S_{7/2} - z^8P^o_{9/2}$) line full-width-of-half-maximum (FWHM) versus delay time (Fig. 2a) and CH_4 pressure (Fig. 2b). FWHM decreases rapidly with increasing delay time. In the same time, the level of background emission is decreasing too, as can be seen from the inset of Figure 2a. FWHM is larger at delay time $\delta = 0$ ns than for $\delta = 200$ ns, and this is valid for each measured CH_4 pressure, as can be seen from Figure 2b. In a dense sample such as ablation plume at initial stages, different line broadening mechanisms, such as Doppler and Stark, contribute to a measured line profile. In the early stage of plume evolution, ionic and electron densities are very large, and we expect significant contribution to the line shape from Stark broadening mechanism [11]. In the present experiment, complete plume emission is coupled into fiber and monochromator, so photons emitted by atoms with very different velocities are collected. This atomic velocity distribution is responsible to Doppler broadening mechanism and, together with Stark broadening, results in observed line shape. As seen from Figure 2a, after approximately 150 ns, measured linewidths do not change significantly, due to the plume cooling and thermalization on background conditions.

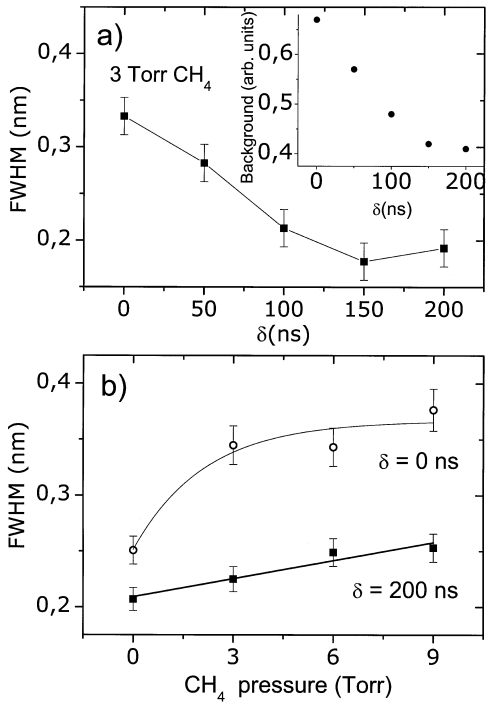

Fig. 2. Full width of half maximum for atomic Mn($e^8S_{7/2}$–$z^8P^o_{9/2}$) line at 482.35 nm in dependence of (a) delay time δ and (b) CH_4 background pressure for two different delays: δ = 0, 200 ns. Line in (a) is only for eye-guiding. Inset in (a) part shows continuum background intensity in dependence of delay time δ. Lines showed in (b) are fit of the obtained FWHM values on exponential growth and linear function, respectively.

3.2 Absorption measurements

While emission was measured summing over the whole plume volume, cavity losses were measured at different distances of the target surface from the cavity axis, thus allowing spatial analysis of ablation plumes. Typical ringdown curves at several wavelengths are shown in Figure 3. Ringdown curve at the wavelength off resonance (empty cavity) is straight line in ln-lin graph. Ringdown curves at laser wavelengths, resonant with the given spectral features, show several characteristic time intervals, due to time dependent absorption [10,12]. In the first time window ablated particles did not reach the cavity axis. As the cloud of atoms and molecules passes through the cavity axis, complicated time dependence of ringdown curves were observed. As the cloud is gone, the slope of the ringdown curve resembles that of the empty cavity. We found that to be true for absorptions at Mn and MnH, while not for C_2 which presence prolongs to much larger time interval. This indicated different production mechanism for C_2.

Figure 4 shows cavity losses in the range 472–482 nm, measured in subsequent time windows in the presence of 0.57 Torr CH_4 (steady condition). Each of subsequent time windows last for 0.5 μs. Cavity loss determined in the first time window, (0.25–0.75) μs, is shown in Figure 4a. We identified observed lines as Mn atomic transitions. In the

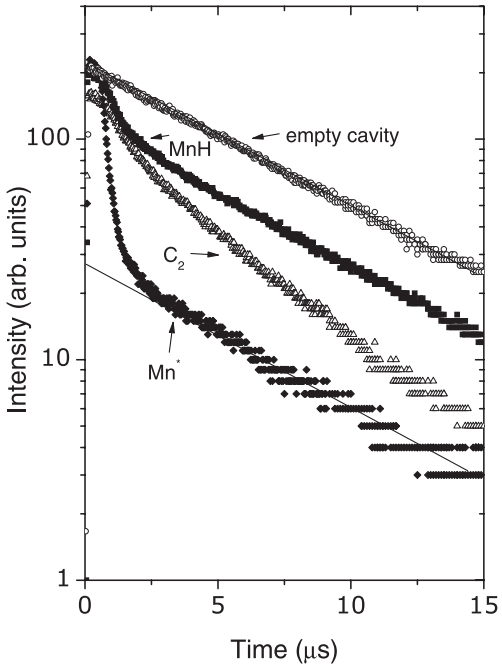

Fig. 3. Typical ringdown transients, in ln-lin scale, for several dye laser wavelengths: laser wavelength off resonance (empty cavity), MnH molecular transition, C_2 molecular transition and atomic Mn transition, as indicated. Empty cavity ringdown transient is approximately described by single-exponential function, which is shown by straight line.

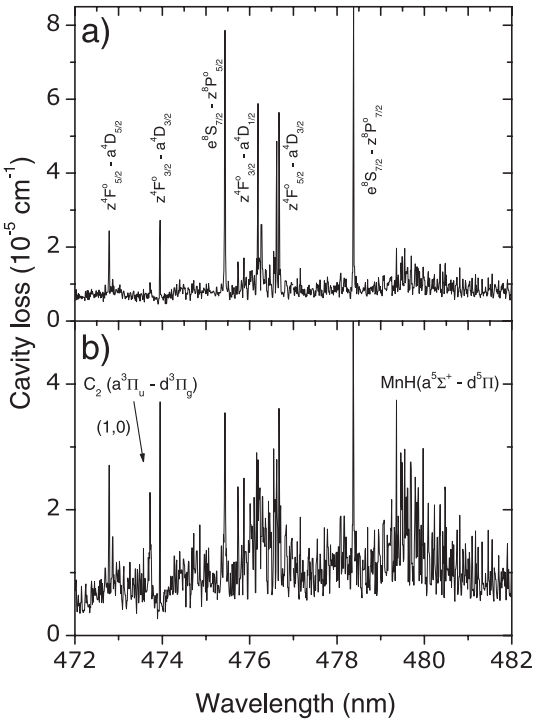

Fig. 4. Cavity losses determined in two subsequent time windows, measured in manganese ablation plume in 0.57 Torr CH_4: (a) time window (0.25–0.75) μs, (b) (0.75–1.25) μs. Distance between target surface and the cavity axis was 0.5 cm and ablation laser fluence 1.6 Jcm^{-2}.

second time window (0.75–1.25) μs, Figure 4b, C_2 (1,0) band within the ($d^3\Pi_g - a^3\Pi_u$) electronic transition is observed [12], together with atomic Mn transitions and intensive band around 480 nm. Absorption could be analyzed further on after 1.25 μs only for losses less than about 5×10^{-5} cm^{-1}. For larger losses, all cavity photons were absorbed in earlier time windows. There are three classes of particles in ablation plume: electrons, ions and neutrals. According to nanosecond laser ablation model, velocities of electrons and ions are in general an order of magnitude larger than accompanying neutrals. In the early time window, Figure 4a, and chosen wavelength interval, we observed mainly neutral Mn atomic transitions. In addition, small absorption losses corresponding to C_2 band head at 474.75 nm were detected. In the following time interval, Figure 4b, C_2 absorption increases. Intensities of all Mn atomic lines decrease and MnH band, situated around 480 nm, is more pronounced. This increase of C_2 absorption in late time window is indication of methane decomposition, for which certain amount of time is required. Among methane decomposition products are free hydrogen atoms which may contribute to MnH formation. Under the action of fast electrons and UV laser light, it is possible to induce decomposition of CH_4 to radicals such as CH_3, CH_2, CH, C, simply by hydrogen extraction. In laser vaporization, presence of large molecules and particulates may contribute to additional scattering losses in the CRD spectrometer. However, these losses are not wavelength dependent and are contributing to the flat background which changes by 2×10^{-6} cm^{-1} for time intervals of Figures 4a and 4b.

Part of the spectrum around 480 nm was measured more carefully in the presence of CH_4. Figure 5 shows spectrum of the manganese ablation plume in the wavelength range (479–481.8) nm. Pressure was 2.8 Torr CH_4, distance of the target surface from the cavity axis was 0.2 cm and fluence 0.8 J cm^{-2} (focus on the target surface). In this spectral region the MnH ($a^5\Sigma^+ - d^5\Pi$) electronic transition is dominant. Signal to noise ratio in showed spectrum is satisfactory good, and even lines with small intensity can be identified. The spectrum has very complex appearance. We indicated only a few most intense ro-vibrational transitions. Identification was performed with the help of tabulated rotational lines within (0,0) and (1,1) and the (2,2) bands of the MnH ($a^5\Sigma^+ - d^5\Pi$) electronic transition [13]. $Q(J)$ progressions indicated in Figure 5 belong to the (0,0) band. In the given wavelength range, $P(J)$ progressions within (0,0), (1,1) and (2,2) bands are present as well. Intensities of identified MnH ro-vibrational lines are now larger than those presented in Figure 4b. As was already mentioned, spectrum showed in Figure 5 was taken under 2.8 Torr CH_4, which is about 1.5 times larger than background pressure for spectrum presented in Figure 4b. Visual inspection shows that ablation plume is of conical shape when it spreads into vacuum. This shape changes into spherical, occupying much smaller volume, in the case of background gas. Increasing background pressure, sphere is becoming smaller, thus inducing increase in number density of ablated material. Three-body collisions are then more probable, with higher efficiency in MnH production. There are two main reasons to believe that MnH molecules are formed in interaction with methane dissociation product: first, we did not observed MnH molecules under vacuum condition and second, intensity of MnH rovibrational lines increase with increasing methane pressure.

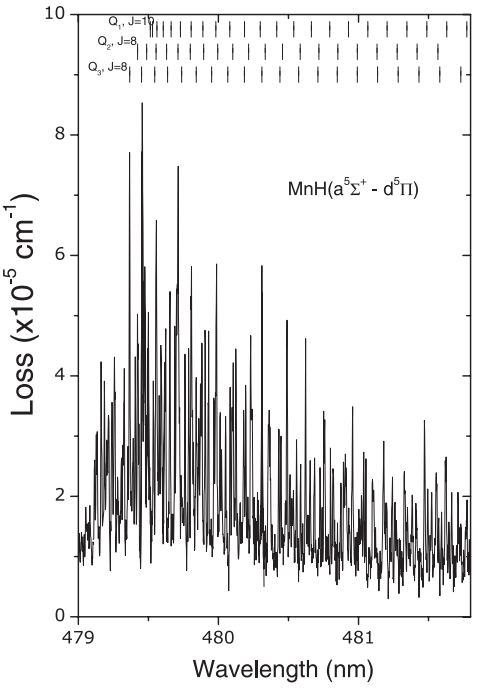

Fig. 5. Absorption loss in the wavelength interval (479–481.8) nm of Mn ablation plume in 2.8 Torr CH_4, showing part of the 480 nm MnH band. Distance between cavity (observation) axis and target surface was 0.2 cm, laser energy 8 mJ, 0.8 J cm^{-2} (focus on the target surface). Observed spectral lines are identified as ro-vibrational transitions of MnH($a^5\Sigma^+ - d^5\Pi$) electronic transition [13]. Indicated Q transitions are within the (0,0) band and P transitions within the (2,2) band.

Figure 6 shows direct comparison of emission and absorption spectra in the same wavelength interval and similar experimental conditions. Figure 6a, shows emission for two different delay times, $\delta = 0$ ns (bold line) and $\delta = 200$ ns (normal line), with the gate of 200 ns. Figure 6b shows cavity loss determined in the time window (0.2–0.44) μs recorded at 2 mm distance of the target surface from the cavity axis. Laser fluence was 0.9 J cm^{-2}. Both emission and absorption were measured in the presence of 3 Torr of methane gas. Overall look on (a) and (b) part of Figure 6 leads to the conclusion that quite different information are obtained from the absorption and the emission spectrum. Manganese atomic lines are spectrally much more narrower in absorption than in emission spectra. Causes of this difference are several. As we already mentioned, emission spectrum is integrated signal over whole plume volume, without taking care of spatial resolution. Instead, we coupled complete plume emission by mirror and lens system into optical fiber and later in

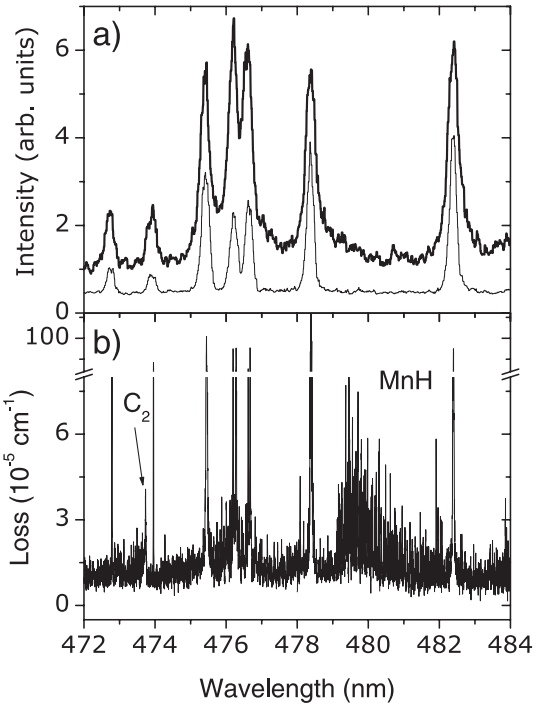

Fig. 6. Comparison of emission and absorption spectra. Methane background pressure was 3 Torr. (a) Emission spectra for two different delay times, 0 ns (bold line), 200 ns (thin line), with gate equal to 200 ns. (b) Absorption loss spectrum taken at 2 mm distance of the target surface from the cavity axis and for 0.9 J cm^{-2} laser fluence. Time window chosen for the loss evaluation was (0.2–0.44) μs.

monochromator. In this way, regions of very different temperatures were included and atoms with very different velocities and moving directions, contribute to final emission line profiles. CRDS spatial resolution is defined by the waist of the laser light in the optical resonator. Absorption spectra are integrated along the line, also including regions of different temperatures, but we implicitly assume that the temperature is constant across the plume, in the cavity axis direction, which is common assumption in successful theoretical models of nanosecond excimer induced plumes [14]. This difference will be discussed in more details below. In addition, by CRDS, we were able to detect not only the excited constituents of ablation plume, but also the ground state atoms and molecules.

Analyzing ringdown transients for particular laser wavelength, we were able to measure velocities of molecules in ablation plume. We define arrival time for different distance along target normal as a point when slopes of ringdown curves off- and on- resonance become different [3,10]. By plotting arrival time versus distance along target normal, we determined velocities of MnH and Mn. Using, so called drag-force model [15], we determined initial velocities of ablated Mn atoms in 1 and 3 Torr of methane background and laser fluence of 0.7 J/cm^2, as 1.1×10^6 cm/s and 7.7×10^5 cm/s, respectively. Determined velocity of MnH molecules in 3 Torr of methane and same laser fluence is 6×10^5 cm/s.

4 Discussion

When ablation plume spreads in the presence of background gas interactions between ablated material and background molecules are possible. Interaction of a nanosecond laser pulse with solid material is complicated process and is divided in three phases: first, photon energy is absorbed by electrons in a bulk. Electrons are thermalized by lattice, surface is melted and evaporation starts. Electrons are coming out from the surface with the highest velocity, followed by ions and neutrals. Dense and hot plume is formed above the target surface within a few picoseconds. This plume spreads isothermally until the termination of the nanosecond laser pulse. In this second phase many post-ionization processes and different collisions are probable. In the third phase, after termination of laser pulse, plume spreads adiabatically in vacuum or background, with the preferred velocity component along the target surface normal. Expansion of the plume is jet-like. Due to the highest velocity, energetic electrons from the bulk start interaction and collisions with background molecules. We believe that electron induced decomposition of methane is a key point in the present experiment, leading to formation of different molecules, like C_2 and MnH. Methane decomposition is followed by hydrogen atom abstraction and addition processes involving background decomposition products and ablated atoms.

We have observed the C_2 and MnH molecules in absorption spectra taken in methane background, as can be seen in Figures 4b, 5 and 6b. The most probable origin of the C_2 molecule are reactions between radicals formed under decomposition of methane. C_2 molecules were observed in the presence of CH_4 regardless of the target used for ablation. We checked it by measuring absorption of magnesium and lithium plumes in the presence of methane, under the same experimental conditions where we have observed the same rovibrational band within the C_2 ($d^3\Pi_g - a^3\Pi_u$) electronic transition. There are several possible methane decomposition paths, such as dissociation under interaction with energetic electrons or photodissociation. Probability for direct photodissociation by the 308 nm laser photons is rather small in our experiment due to the wavelength limit ($\sim$277 nm for CH_3 + H decomposition [16]) and laser fluence which is not high enough for two-photon process. Interactions of CH_4 with energetic electrons were studied and modelled, in dependence on electron energy, gas density [17–19]. Methane molecules decompose into CH_3, CH_2, CH and C under action of fast electrons. The electron energy required for methane dissociation is approximately 10 eV [20]. Measured manganese atoms velocities correspond to energy of about 30 eV. Keeping in mind that velocity of electrons in nanosecond laser pulse induced plume is higher than neutral particle velocities [21], we concluded that electrons possess enough energy to induce decomposition of methane. Beside neutral decomposition products, CH_n^+ ions are also possible products of photoionization of neutral CH_n, $n = 1...4$ [22].

Dissociation products mentioned above and free hydrogen atoms can react with the ablated Mn atoms and form

the MnH molecule. The electronic ground state of MnH is of the $X^7\Sigma$ symmetry, while observed MnH spectrum belongs to the $d^5\Pi_i \leftarrow a^5\Sigma^+$ electronic system. Bands corresponding to electronic transition from the ground state $X^7\Sigma$ to the first electronic excited $A^7\Pi$ state were not accessible with our CRD spectrometer (for example (0,0) band lies around 568 nm [23]). Metastable $a^5\Sigma^+$ electronic state is for 3358 cm^{-1} shifted from the electronic ground $X^7\Sigma$ state, while the shift for $d^5\Pi_i$ is 20880.56 cm^{-1}. Knowledge about this latter state is rather poor: molecular constants were determined [13] while no accessible data on potential energy function nor dipole moments for $d^5\Pi_i$ state exists [24,25]. We assume that MnH is formed in collisional process

$$\mathrm{Mn + H + X \rightarrow MnH}(a^5\Sigma^+) + \mathrm{X} \qquad (1)$$

where X is third body taking care of extra momentum. Beside direct collisional process 1, alternative reaction could be

$$\mathrm{Mn + CH}_n \rightarrow \mathrm{MnH + CH}_{n-1}, \quad n = 1...4, \qquad (2)$$

or similar one involving CH_n^+ ions. For $n = 4$, process 2 is exothermic with $\Delta E \sim 16539$ cm^{-1}: binding energy of CH_4 is 36100 cm^{-1} for decomposition on products H + CH_3 [16], while binding energy of MnH is approximately 19560 cm^{-1} [26]. MnH molecules are usually generated in various electrical discharges or King furnace and detected in emission or absorption [13,23,24,27]. Laser ablation of solid Mn target in CH_4 background presented here can be considered as analogous generation process. CRDS setup used for this work and laser ablation of manganese target in methane atmosphere, could be useful tool for further MnH spectroscopy. It is known that different mechanisms influence the line shape in discharges leading to spectral line overlap and decreased resolution. With use of the CRDS detection in ablation plume, such problems are greatly reduced. In the laser plume, ablated particles move normally to the target surface, with small tangential velocity components. In this experiment, we measured absorption perpendicular to the moving direction where Doppler broadening is significantly reduced. This fact can be used to explain much narrower lines in absorption spectra as compared to broad lines in emission spectra. Advantage of absorption measurements over emission is best illustrated in Figure 6, where we directly compared both results. Using CRDS, we were able to detect C_2 and MnH transitions, while in emission this was not the case.

Natural linewidths for observed Mn atomic transitions are equal to several MHz [28], while calculated Doppler linewidths for temperatures of about 3000 K (as determined in Ref. [7]) are of about several GHz. Measured linewidths for transitions presented in Figures 1 and 2 are much larger (order of magnitude 100 GHz), indicating role of other broadening mechanisms, like Stark. Influence of Stark broadening in early stage of plume expansion is particularly strong due to high density of charged contents of the plume.

On the other hand, manganese atomic line transitions are much narrower when measured by CRDS. By employing CRDS perpendicularly to the species moving in a sort of beam expansion, Doppler broadening is minimized. Stark broadening, important in very early stage of the plume expansion is reduced in absorption spectra due to a certain delay time, at which spectra are taken, relative to the vaporization starting point.

Dye laser FWHM is equal to 6 GHz, which is larger than linewidths of reported absorption spectral features. According to conclusions given in reference [29], for absorbances sufficiently small (as in the present case), behavior of ringdown curves is nearly exponential and one is able to extract the exact absorption.

Emission spectroscopy can be applied to study plume with zero delay after ablation laser pulse, but without ability to detect species in ground and metastable states. CRDS is very useful technique for plume study in later times, especially for detection of molecules formed in various interactions of plume contents with background. Unfortunately, performing of CRDS in very early times of plume evolution and closer to target is not possible due to increase of near surface cavity losses and scattering of cavity photons [30].

5 Conclusions

We analyzed Mn ablation plume in vacuum and methane background by optical gated emission spectroscopy and cavity ringdown spectroscopy. Gated emission spectroscopy allows us to detect plasma emission from the early beginning of its development, while by CRDS we were able to detect absorption only in times after arrival of ablated material to the cavity axis. In emission spectra, we observed broad continuum and numerous Mn atomic transitions, both in vacuum and in the presence of methane. In absorption spectra we observed also atomic Mn transitions, and in the presence of methane also C_2 and MnH molecules. We showed that complete picture of manganese ablation plume is obtained by combining emission and absorption measurements.

This work was financially supported by the Ministry of Science, Education and Sports of the Republic of Croatia, project #0035003.

References

1. E. Tognoni, V. Palleschi, M. Corsi, G. Cristoforetti, Spectrochim. Acta Part B **57**, 1115 (2002)
2. G. Berden, R. Peeters, G. Meijer, Int. Rev. Phys. Chem. **19**, 565 (2000)
3. I. Labazan, S. Milošević, Chem. Phys. Lett. **352**, 226 (2002)
4. V. Bulatov, A. Khalmanov, I. Schechter, Anal. Bioanal. Chem. **375**, 1282 (2003)
5. S. Hasegawa, A. Yamasaki, A. Suzuki, Appl. Surf. Sci. **161**, 323 (2000)
6. P. Lecoeur, A. Gupta, P.R. Duncombe, G.Q. Gong, G. Xiao, J. Appl. Phys. **80**, 513 (1996)

7. H.J. Dang, Z.H. Han, Z.G. Dai, Q.Z. Qin, Int. J. Mass Spectrom. **178**, 205 (1998)
8. R.O. Gray, *A digital spectral clasification atlas*, `http://nedwww.ipac.caltech.edu/level5/Gray/Gray_contents.html`
9. S. Gogić, S. Milošević, Fizika A **7**, 37 (1998)
10. I. Labazan, S. Milošević, Phys. Rev. A **68**, 032901 (2003)
11. I. Labazan, S. Milošević, J. Phys. D: Appl. Phys. **37**, 2975 (2004)
12. I. Labazan, N. Krstulović, S. Milošević, J. Phys. D: Appl. Phys. **36**, 2465 (2003)
13. W.J. Balfour, B. Lindgren, O. Launila, S. O'Connor, E. J. Cusack, J.Mol. Spectrosc. **154**, 177 (1992)
14. R.K. Singh, J. Narayan, Phys. Rev. B **41**, 8843 (1990)
15. H. Chae, S.M. Park, Bull. Korean Chem. Soc. **18**, 448 (1997)
16. P.A. Cook, M.R.N. Ashfold, Y.-J. Jee, K.-H. Jung, S. Harich, X. Yang, Phys. Chem. Chem. Phys. **3**, 1848 (2001)
17. H.F. Winters, J. Chem. Phys. **63**, 3462 (1975)
18. K. Tachibana, M. Nishida, H. Harima, Y. Urano, J. Phys. D: Appl. Phys. **17**, 1727 (1984)
19. M. Heintze, M. Magureanu, M. Kettlitz, J. Appl. Phys. **92**, 7022 (2002)
20. M. Heintze, M. Magureanu, J. Appl. Phys. **92**, 2276 (2002)
21. V. Berardi, S. Amoruso, N. Spinelli, N. Armenante, R. Velotta, F. Fuso, M. Allegrini, E. Arimondo, Int. J. Mass Spectrom. Ion Proc. **144**, 1 (1995)
22. K.N. Joshipura, M. Vinodkumar, B.K. Antony, N.J. Mason, Eur. Phys. J. D **23**, 81 (2003)
23. T.D. Varberg, R.W. Field, A.J. Merer, J. Chem. Phys. **95**, 1563 (1991)
24. W.J. Balfour, J. Chem. Phys. **88**, 5242 (1988)
25. S.R. Langhoff, C.W. Bauschlicher Jr, A.P. Rendell, J. Mol. Spectrosc. **138**, 108 (1989)
26. `http://www.webelements.com/webelements/elements/text/Mn/enth.html`
27. W.J. Balfour, O. Launila, L. Klynning, Mol. Phys. **69**, 443 (1990)
28. W.C. Martin, J.R. Fuhr, D.E. Kelleher, A. Musgrove, L. Podobedova, J. Reader, E.B. Saloman, C.J. Sansonetti, W.L. Wiese, P.J. Mohr, K. Olsen, NIST *Atomic Spectra Database (version 2.0), [Online]. Available:* `http://physics.nist.gov/asd` National Institute of Standards and Technology, Gaithersburg, MD (1999)
29. P. Zalicki, R.N. Zare, J. Chem. Phys. **102**, 2708 (1995)
30. M. Zhao, E.H. Wahl, T.G. Owano, C.C. Largent, R.N. Zare, C.H. Kruger, Chem. Phys. Lett. **318**, 555 (2000)